The elastochrone: the descent time of a sphere on a flexible beam

By Jeffrey M. Aristoff[1], Christophe Clanet[2]
and John W. M. Bush[1],*

[1]*Department of Mathematics, Massachusetts Institute of Technology, Cambridge, MA 02139, USA*
[2]*Department of Mechanics, École Polytechnique, 91128 Palaiseau, France*

We present the results of a combined experimental and theoretical investigation of the motion of a sphere on an inclined flexible beam. A theoretical model based on Euler–Bernoulli beam theory is developed to describe the dynamics, and in the limit where the beam reacts instantaneously to the loading, we obtain exact solutions for the load trajectory and descent time. For the case of an initially horizontal beam, we calculate the period of the resulting oscillations. Theoretical predictions compare favourably with our experimental observations in this quasi-static regime. The time taken for descent along an elastic beam, the elastochrone, is shown to exceed the classical brachistochrone, the shortest time between two points in a gravitational field.

Keywords: moving load; flexible beam; brachistochrone

1. Introduction

In the early seventeenth century, Galileo Galilei built an inclined ramp on which he rolled spheres of different size and density (Galilei 1638). From his measurements, he deduced a relationship between the sphere's position and the elapsed time, and so inferred the apparent constancy of the Earth's gravitational acceleration. Galileo also argued that the path of quickest descent between two points would be an arc of a circle, but as demonstrated by Johann and Jakob Bernoulli, Leibniz and arguably Newton (Anon 1697), such a path was found instead to be an inverted cycloid, the travel time along which corresponds to the brachistochrone (Boyer & Merzbach 1991). We here consider a variation of Galileo's study in which the rigid ramp is replaced by a flexible beam that can bend under its own weight and that of the rolling sphere.

A fundamental understanding of the dynamic behaviour of flexible beams subjected to moving loads is central to the design of many engineering structures, including bridges and railways. Aspects of this problem have been studied extensively, beginning with Stokes (1849), Willis (1849) and Zimmermann (1896), who considered a beam with negligible mass traversed by a single load moving at constant speed. Subsequently, Krylov (1905), Timoshenko (1908) and

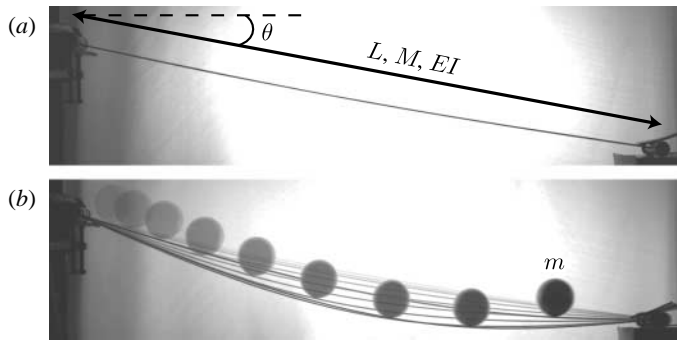* Author for correspondence (bush@math.mit.edu).

Figure 1. (*a*) Photograph of a simply supported metre-long beam with mass $M=0.33$ kg, stiffness $EI=4.03$ kg m^3 s^{-2} and initial inclination $\theta=10.0°$. (*b*) Overlaid images taken at 0.1 s intervals following the release of a 2.5-in. diameter steel sphere weighing $m=1.0$ kg onto the beam. $\mathcal{M}=m/M=3.14$, $\mathcal{K}=MgL^2/EI=0.744$.

Lowan (1935) investigated the limit where the load mass is negligible relative to that of the beam. Steuding (1934), Schallenkamp (1937) and Bolotin (1961) and others included both the beam and load mass in their analysis of loads moving at constant speed. The generalization to load motion at variable but deflection-independent acceleration has received recent attention, and is discussed for example by Lee (1995) and Michaltsos (2002).

One-dimensional elements resistant to tension but not to bending, such as strings, cables, chains and ropes, are frequently used in modern structures. Vibration studies of these elements subjected to moving loads began with Smith (1964), who studied the motion of a mass moving at constant speed along a stretched string. Flaherty (1968), Sagartz & Forrestal (1975) and Rodeman *et al.* (1976) considered variable-speed load motion, and Derendyayev & Soldatov (1997) and Blinov (2008) included the load's inertia. For a comprehensive review of the dynamic response of solid structures under moving loads, see for example Fryba (1972), or from a historical viewpoint, see Timoshenko (1953).

Civilian and military operations on floating ice are common in Arctic regions and have motivated a number of scientific studies. Kerr (1976) surveyed early research on the response of floating ice to static loads. Nevel (1970) considered the local stresses generated by a load moving at constant speed, and Davys *et al.* (1985) analysed the far-field wave patterns. Considerable effort has been made to predict the critical load speed, above which flexural-gravity waves can propagate freely, and below which no such waves are generated (e.g. Hosking *et al.* 1988; Strathdee *et al.* 1991). For a review of the modern theory of moving loads on ice plates, see Squire *et al.* (1996) and references therein.

In all previous studies of beams, the load speed or acceleration is prescribed and independent of the resulting deflection, but in general this need not be the case. Consider the motion of a solid steel sphere with mass m along a simply supported flexible beam with length L, mass M, Young's modulus E, area moment of inertia I, stiffness EI and initial beam inclination θ, as depicted in figure 1. Provided the beam is inextensible, the system may be characterized by three dimensionless groups: the load-to-beam mass ratio $\mathcal{M}=m/M$; the initial beam inclination θ; and the torque ratio $\mathcal{K}=MgL^2/EI$, which represents the tendency of the beam to bend under its own weight (g is the gravitational acceleration).
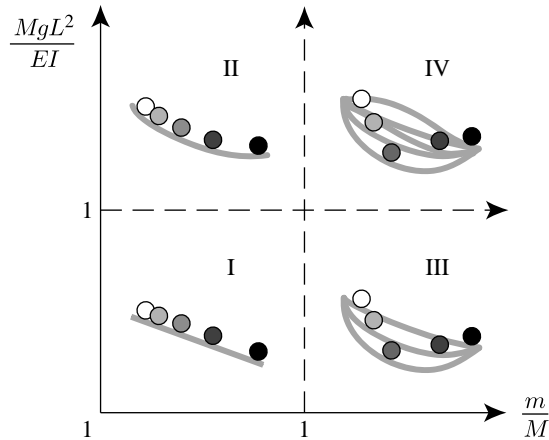
Figure 2. Regime diagram depicting the beam-and-mass dynamics and indicating the scope of the present study (regions II, III and IV).

This classification allows us to identify four regions in the phase space $(\mathcal{M}, \mathcal{K})$ as shown in figure 2. Region I ($\mathcal{K} \ll 1$, $\mathcal{M} \ll 1$) corresponds to Galileo's rigid ramp and a uniformly accelerated sphere. In region II ($\mathcal{K} \gg 1$, $\mathcal{M} \ll 1$) the beam bends under its own weight, independent of the sphere dynamics. In region III ($\mathcal{K} \ll 1$, $\mathcal{M} \gg 1$), the beam does not deform under its own weight, but rather under the weight of the sphere, and the beam shape is thereby coupled to the sphere dynamics. In region IV ($\mathcal{K} \gg 1$, $\mathcal{M} \gg 1$), the beam bends under its own weight and that of the sphere, and one expects that the beam's inertia may generate waves as the sphere rolls. In the present study, we consider the system dynamics in regions II, III and IV, where the sphere acceleration is deflection dependent.

Further insight into the beam-and-mass dynamics may be obtained by considering the characteristic length scales and time scales associated with the load motion. Along an initially horizontal beam, the characteristic deflection length scale ϵ is found by equating the bending energy $EI(\epsilon/L^2)^2 L$ to the gravitational potential energy $\epsilon(m + M)g$, yielding

$$\epsilon \sim \frac{(m + M)gL^3}{EI}, \tag{1.1}$$

that corresponds to the maximum static deflection. The characteristic load speed is thus $U \sim \sqrt{\epsilon g}$, and the time scale associated with the load motion is therefore

$$T_1 \sim L/U \sim \sqrt{\frac{EI}{(m + M)g^2 L}}. \tag{1.2}$$

Along a rigid beam with inclination θ, vertical motion occurs over a length scale $L \sin \theta$ and a time scale

$$T_2 \sim \sqrt{\frac{L}{g \sin \theta}}.$$

For $T_1 \ll T_2$ or equivalently $\mathcal{K}(1 + \mathcal{M}) \gg \sin \theta$, the beam deflection is principally responsible for load motion, while for $T_1 \gg T_2$, the initial inclination provides the impetus.

A third time scale, the reaction time T_b of the beam to an applied load, may be estimated by comparing the kinetic energy of the beam $M(\epsilon/T_b)^2$ to the bending energy. Doing so yields

$$T_b \sim \sqrt{\frac{ML^3}{EI}}. \tag{1.3}$$

Provided the relevant time scale of load motion $\min(T_1, T_2) \gg T_b$, the beam adapts instantaneously to the loading. We shall primarily be interested in this quasi-static limit arising when

$$\begin{cases} \mathcal{K} \ll \csc\theta, & \text{for } T_1 \gg T_2, \\ \mathcal{K} \ll (1+\mathcal{M})^{-1/2}, & \text{for } T_1 \ll T_2. \end{cases} \tag{1.4}$$

Both the load's inertia and weight contribute to the beam deflection, the ratio of which is prescribed by the Froude number $\mathcal{F} = U^2/(gR_c \cos\theta)$ where $R_c = L^2/\epsilon$ is the characteristic radius of curvature of the beam. One may thus neglect the load's inertia provided $\mathcal{F} \ll 1$, or equivalently

$$\begin{cases} \dfrac{\epsilon}{L} \ll \cot\theta, & \text{for } T_1 \gg T_2, \\ \left(\dfrac{\epsilon}{L}\right) \ll \sqrt{\cos\theta}, & \text{for } T_1 \ll T_2. \end{cases} \tag{1.5}$$

Note that $\mathcal{F}$ is not an independent parameter, but instead depends explicitly on $\mathcal{K}$, $\mathcal{M}$ and θ through (1.1).

In §2 we describe our experimental technique and report our observations. In §3 we develop a theoretical model for the beam-and-mass dynamics, and deduce the travel time along a flexible ramp, the elastochrone. Particular attention is given to the quasi-static limit in which an analytical expression for the load trajectory and descent time may be obtained. The value and limitations of our model are discussed in §4.

2. Experiment

The beam used in our study is 0.96 m long, 5.0 cm wide, 2.5 mm thick, weighs 0.33 kg, and is constructed from an aluminium grade 6061 T6 standard rule. The stiffness of the beam is determined by clamping it to a level surface at various distances from its free end, and measuring the tip deflection. The data are then compared to the deflection predicted by nonlinear beam theory, and the best-fit value for the stiffness is found to be $4.03 \pm 0.12\ \text{kg m}^3\,\text{s}^{-2}$, yielding $\mathcal{K} = MgL^2/EI = 0.744$. For the remaining experiments, each end of the beam is attached to a pair of ball bearings in such a way that the beam is free to rotate. At the upper end of the beam, the bearings are clamped to a support, and at the lower end, the bearings rest on a level surface. Fixed- and hinged-end boundary conditions are thus obtained. Each support weighs 0.011 kg and has a rotational inertia of $3.38 \times 10^{-6}\ \text{kg m}^2$. A digital level, accurate to $\pm 0.05°$, is used to measure the initial inclination of the beam.
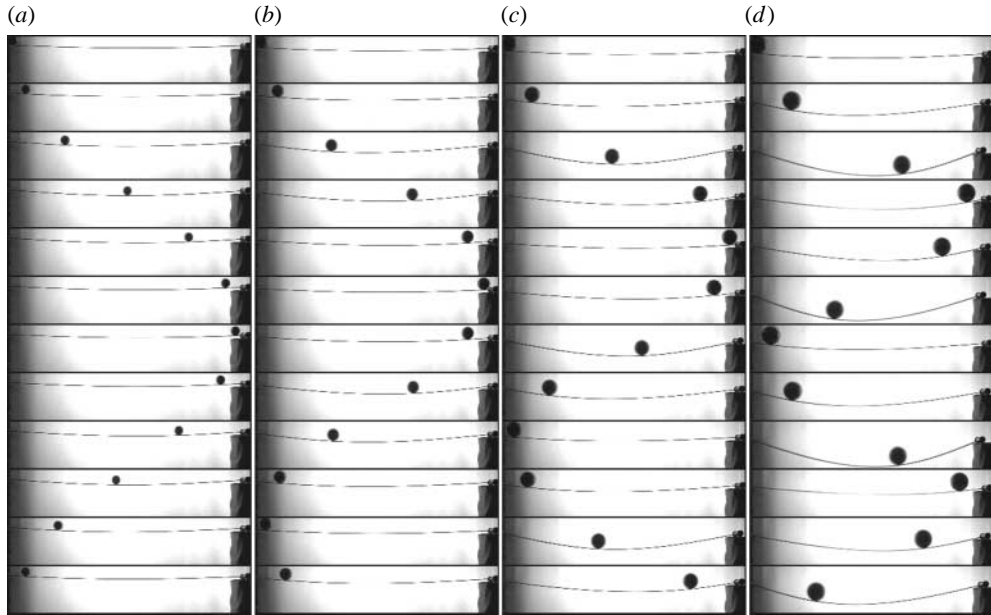
(*a*) (*b*) (*c*) (*d*)

Figure 3. Image sequences showing the first 7.2 s following the release of steel spheres of different masses onto a metre-long initially horizontal beam. The time between images is 0.6 s. (*a*) 1.5 in. diameter sphere, $\mathcal{M}=0.68$; (*b*) 2.0 in. diameter sphere, $\mathcal{M}=1.61$; (*c*) 2.5 in. diameter sphere, $\mathcal{M}=3.14$; (*d*) 3.0 in. diameter sphere, $\mathcal{M}=5.43$.

Nine steel spheres (density $7700 \, \text{kg m}^{-3}$) are used in the experiment. The diameters of the steel spheres range from 1 to 3 in. in increments of quarter inches, corresponding to a nearly 10-fold variation in mass, from 0.22 to 1.8 kg. The spheres traverse the beam lengthwise, rolling along a shallow groove cut into the beam, 0.76 mm deep and 4.6 mm wide, which prohibits the spheres from moving laterally. While movement of the supports gives rise to friction, it may be neglected on the grounds that the rotational and translational inertia of the supports are negligible relative to those of the sphere and beam, respectively.

An experiment is initiated by placing the sphere at the desired starting position. The sphere is then released from rest and its motion recorded at $200 \, \text{frames s}^{-1}$ using a high-speed video camera. A typical resolution of $1 \, \text{pixel mm}^{-1}$ in 32-bit greyscale is obtained. Backlighting provides sufficient contrast to visualize both the beam and sphere dynamics.

A first series of experiments was performed in which each sphere was released from one end of an initially horizontal beam. This series is presented in figure 3. Motion occurs as a result of the unbalanced gravitational force along the tangent to the beam that arises due to the beam bending under its own weight. A periodic motion of the beam-and-mass system is observed: the sphere traverses the beam back and forth, with a period of several seconds. The oscillatory motion continues, and the change in length ℓ of the trajectory over a single period is measured: $\Delta\ell/\ell = (2.4 \pm 1.3)\%$. Thus, we conclude that dissipation due to friction is negligible over a single period. In order to quantitatively summarize the experimental results, we construct a space–time diagram for each experiment. The diagram is constructed by taking a one-pixel-wide vertical
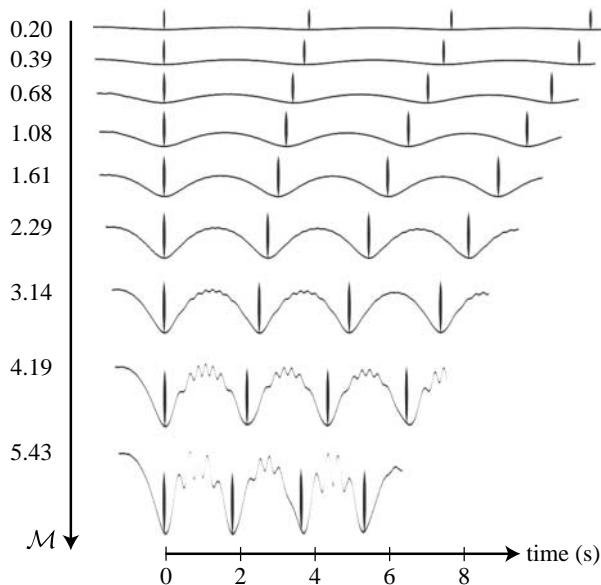
Figure 4. Space–time diagram of the beam's midpoint deflection for increasing load-to-beam mass ratios, $\mathcal{M}$, indicating deflection amplitude, vibration amplitude, vibration frequency and period of sphere motion. The vertical patches correspond to the times when the sphere passes the beam's midpoint. $\mathcal{K} = 0.744$, $\theta = 0$.

slice of each frame, and stacking each slice horizontally. We choose a slice through the beam's midpoint in order to capture the maximum beam deflection, and plot the resulting montage in figure 4 for each experiment. As the mass of the sphere is increased, we observe several key features that we shall rationalize in §3. First, the deflection amplitude increases. Second, the period of load motion decreases from approximately 8 to 4 s. Third, for $\mathcal{M} > 2$, bending waves arise with increasing amplitude and a frequency that decreases from approximately 6 to $4\,\mathrm{s}^{-1}$. The dependence of the deflection amplitude and vibration amplitude on the load-to-beam mass ratio is quantified in figures 5 and 6, respectively.

A second series of experiments was performed in which each sphere was placed at various distances from the midpoint of a beam with endpoints at equal heights, from a position corresponding to the static equilibrium of the bent beam. The sphere was then released, and the periodic motion of the mass and beam again observed. In figure 7, we plot the observed period versus release position, x_0, as measured from the end of the beam. Two trends are readily apparent from the data. First, the period of motion remains nearly constant (within 5% of its average value) for a given mass, provided that the sphere is released sufficiently close to the beam centre, $|x_0/L - 0.5| \leq 0.25$. Second, as the release position departs farther from the beam centre, the period increases, a dependence to be rationalized in §3.

A third series of experiments was performed in which the beam was given an initial inclination $\theta = 10.0°$, and each sphere released 2.5 cm from the upper end of the beam. The resulting motion is shown in figure 8 for three experiments. We observe that as the sphere's weight is progressively increased, the deflection
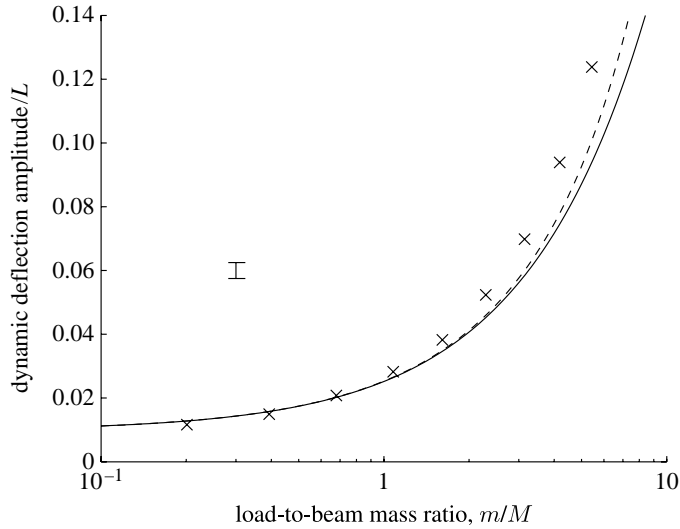
Figure 5. Dimensionless dynamic deflection amplitude versus load-to-beam mass ratio m/M for an initially horizontal beam. The cross marks denote the experimentally observed beam deflections. The solid curve is defined by (3.12) and the dashed curve by (3.24). A characteristic error bar is shown.
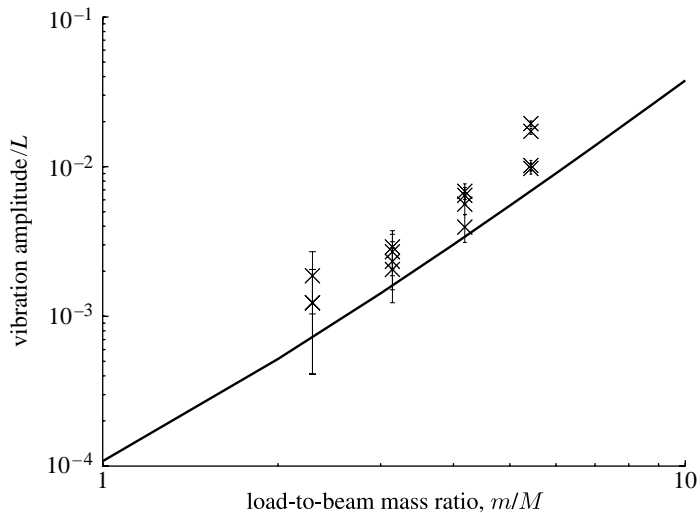

Figure 6. Dimensionless vibration amplitude versus load-to-beam mass ratio for the motion of a sphere along an initially horizontal beam. The cross marks denote the experimentally observed vibration amplitudes. The solid line is given by the difference between the dynamic and static deflections, defined by (3.24) and (3.12), respectively. Characteristic error bars are shown.

amplitude increases and the descent time decreases. In figure 9, we present the descent time τ as a function of sphere weight. The time τ is scaled by the descent time along a rigid beam: $\tau_G = \sqrt{(1 + J/(mR^2))(2l/(g \sin \theta))}$, where $J = (2/5)mR^2$ is the rotational inertia of the sphere, and $l = L - 2.5$ cm the distance travelled. We first note that descent is faster along a flexible than rigid
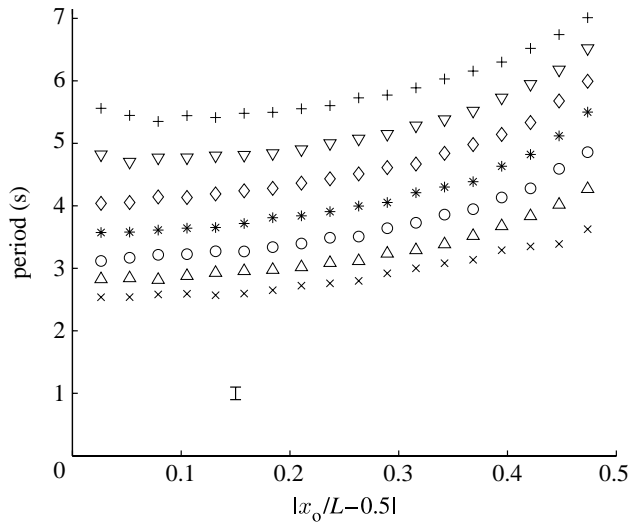
J. M. Aristoff et al.

Figure 7. Period of sphere motion versus release distance from the beam midpoint of an initially horizontal beam for various load-to-beam mass ratios $\mathcal{M} = m/M$: crosses, $\mathcal{M} = 5.43$; up triangles, $\mathcal{M} = 4.19$; circles, $\mathcal{M} = 3.14$; asterisks, $\mathcal{M} = 2.29$; diamonds, $\mathcal{M} = 1.61$; down triangles, $\mathcal{M} = 1.08$; pluses, $\mathcal{M} = 0.68$. A characteristic error bar is shown.

beam. Moreover, we observe that the heavier spheres descend faster, until $\mathcal{M} \approx 5$, beyond which the sphere may lift off the beam before reaching the opposite end. As the load-to-beam mass ratio $\mathcal{M}$ approaches zero, the descent time is observed to approach a constant, since the beam does not bend beneath the weight of the sphere. However, since the beam bends under its own weight, the descent time is still less than that along a rigid incline.

3. Theoretical model

We consider the motion of a rigid sphere with radius R, mass m and rotational inertia J, which traverses a simply supported, inextensible, undamped beam with length $L \gg R$, mass M, stiffness EI and initial inclination θ. The motion takes place in a gravitational field and is depicted in figure 10. Let x denote the coordinate along the line adjoining the beam endpoints, and $w(x, t)$ the beam deflection from this line. Let $s(t)$ denote the position of the sphere. If we assume that the behaviour of the beam is governed by Euler–Bernoulli beam theory, the equation for the beam displacement takes the form:

$$EIw_{xxxx} + \frac{M}{L} w_{tt} = P, \tag{3.1}$$

where $P = P_1 + P_2$ is the loading force per unit length (Fryba 1972), and we have taken the small-slope limit: $w_x \ll 1$. The terms on the left-hand side of (3.1) arise, respectively, from the bending and kinetic energy of the beam, and $P_1 = Mg \cos \theta / L$ is the distributed loading due to the normal component of the beam's weight. Applying D'Alembert's principle and assuming continuous contact between the sphere and beam, the normal component of the sphere's weight gives rise to the loading
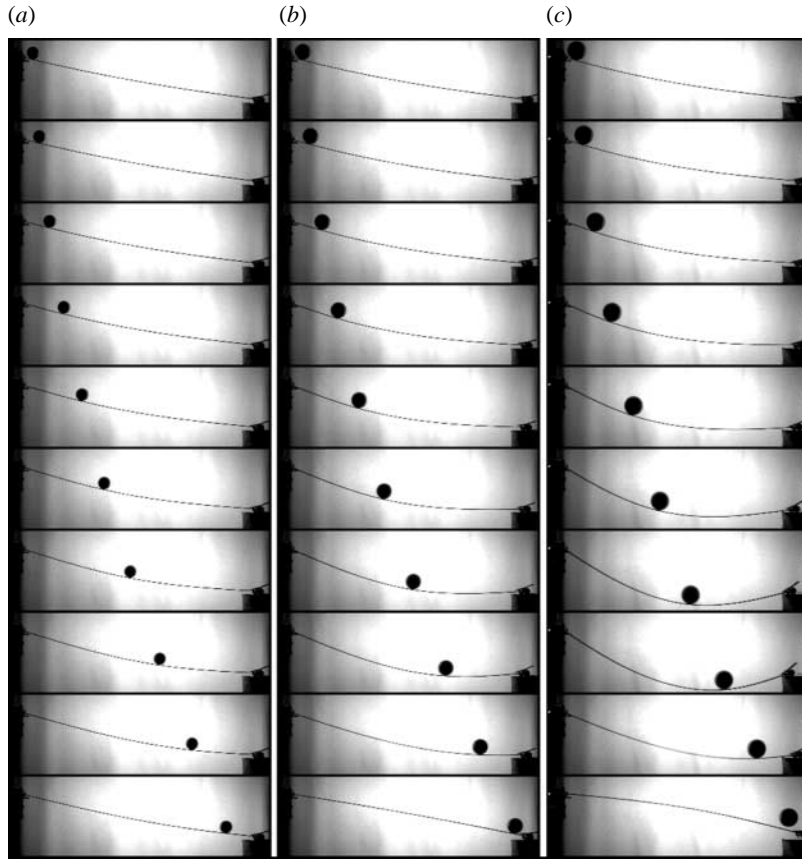
(*a*) (*b*) (*c*)

Figure 8. Image sequences of steel spheres traversing a metre-long beam with initial inclination $\theta = 10.0°$. The time between images is 0.1 s. (*a*) 2.0 in. diameter sphere, $\mathcal{M} = 1.61$; (*b*) 2.5 in. diameter sphere, $\mathcal{M} = 3.14$; (*c*) 3.0 in. diameter sphere, $\mathcal{M} = 5.43$. Note that the sphere has lost contact with the beam in the final image of sequence *c*.

$$P_2 = m\left(g \cos\theta - \frac{\mathrm{d}^2 w(s, t)}{\mathrm{d}t^2} \right) \delta(x - s), \tag{3.2}$$

where $\delta(x - s)$ is the delta function and the term $m(\mathrm{d}^2 w(s, t)/\mathrm{d}t^2)$ accounts for the inertial forces. The appropriate boundary and initial conditions for (3.1) are

$$w(0, t) = w(L, t) = w_{xx}(0, t) = w_{xx}(L, t) = w_t(x, 0) = w_{tt}(x, 0) = 0. \tag{3.3}$$

In appendix A, we justify the use of the small-slope approximation to describe the observed motion.

The motion of the sphere is prescribed by

$$m\frac{\mathrm{d}^2 s}{\mathrm{d}t^2} + m w_{tt} w_x \delta(x - s) = F(t), \tag{3.4}$$

where the second term accounts for the tangential acceleration imparted to the sphere by the beam motion, and $F(t)$ is the tangential forcing. We note that in the engineering literature, $F(t)$ is typically prescribed so as to describe the
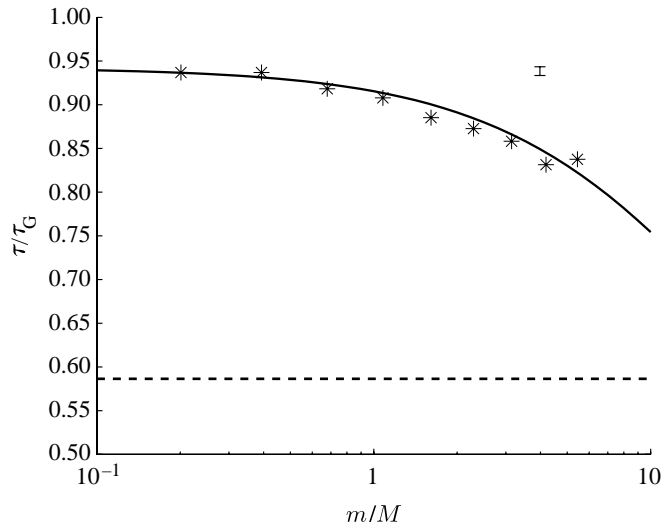
Figure 9. Descent time τ relative to that along a rigid beam, $\tau_G = 1.21$ s, versus load-to-beam mass ratio m/M for loads released 2.5 cm from the top of the beam. The asterisks denote the experimentally observed descent times. The solid curve is determined by numerically integrating (3.16). For comparison, the descent time along the brachistochrone curve (3.21) is given by the dashed line. We note that the quasi-static approximation will fail before the curves intersect. A characteristic error bar is shown. Initial beam inclination $\theta = 10.0°$.
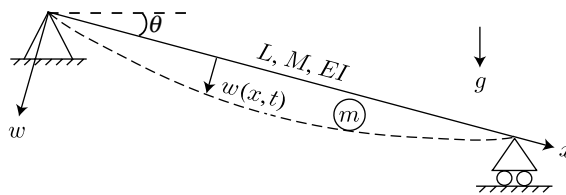

Figure 10. Schematic of a sphere with mass m traversing a simply supported inclined beam having length L, mass M, stiffness EI and initial inclination θ. A particular beam deflection $w(x, t)$ is shown.

motion of a vehicle that is travelling at either constant speed or acceleration (Lee 1995; Michaltsos 2002). Here, $F(t)$ is coupled to the beam so that the sphere acceleration becomes deflection dependent, arising from the unbalanced gravitational force along the tangent to the beam

$$F(t) = mg(\sin\theta + w_x\delta(x-s)\cos\theta) - f. \tag{3.5}$$

The force due to friction f gives rise to rotation of the load, but does not dissipate energy in rolling because the base of the load is at rest at each point of contact with the beam surface. If the load rolls without slipping, a torque balance requires $J\alpha = Rf$, where α is the angular acceleration of the load. Since $d^2s/dt^2 = R\alpha$, we find $f = (J/R^2)(d^2s/dt^2)$. Note that $J = (2/5)mR^2$ if the sphere rolls, and $J = 0$ if it slips.

In §1, we deduced the appropriate time scale for the sphere's motion, $T_{\min} = \min(T_1, T_2)$. Thus, by introducing the dimensionless variables $\bar{x} = x/L$, $\bar{w} = w/\epsilon$, $\bar{s} = s/L$ and $\bar{t} = t/T_{\min}$, (3.1) and (3.2) may be combined and the beam motion described by

$$\frac{\epsilon}{L}\bar{w}_{\bar{x}\bar{x}\bar{x}\bar{x}} + \mathcal{K}\sin\theta\frac{\epsilon}{L}\bar{w}_{\bar{t}\bar{t}} = \mathcal{K}\cos\theta + \mathcal{K}\mathcal{M}L\left(\cos\theta - \sin\theta\frac{\epsilon}{L}\frac{\mathrm{d}^2\bar{w}(\bar{s},\bar{t})}{\mathrm{d}\bar{t}^2}\right)\delta(\bar{x}-\bar{s}),$$

$$(3.6)$$

for $T_1 \gg T_2$, and

$$\frac{\epsilon}{L}\bar{w}_{\bar{x}\bar{x}\bar{x}\bar{x}} + \mathcal{K}^2(1+\mathcal{M})\frac{\epsilon}{L}\bar{w}_{\bar{t}\bar{t}}$$

$$= \mathcal{K}\cos\theta + \mathcal{K}\mathcal{M}L\left(\cos\theta - \mathcal{K}(1+\mathcal{M})\frac{\epsilon}{L}\frac{\mathrm{d}^2\bar{w}(\bar{s},\bar{t})}{\mathrm{d}\bar{t}^2}\right)\delta(\bar{x}-\bar{s}), \qquad (3.7)$$

for $T_1 \ll T_2$, where ϵ is the characteristic deflection ($\epsilon \ll L$).

(a) Quasi-static approximation

Provided the motion is quasi-static as defined by (1.4), and that the load's inertia is small relative to its weight as defined by (1.5), then both (3.6) and (3.7) reduce to

$$\frac{\epsilon}{L}\bar{w}_{\bar{x}\bar{x}\bar{x}\bar{x}} = \mathcal{K}' + \mathcal{K}'\mathcal{M}L\delta(\bar{x}-\bar{s}), \qquad (3.8)$$

where $\mathcal{K}' = \mathcal{K}\cos\theta$. We shall proceed by seeking a solution to (3.8). A correction for the beam shape due to the load's inertia will be presented in §3d.

The delta function in (3.8), which corresponds physically to a discontinuity in the shearing force, obliges us to solve for the shape of the beam separately on either side of the load. For $0 \leq \bar{x} < \bar{s}$, we obtain the beam shape via integration of (3.8):

$$\frac{\epsilon}{L}\bar{w}_1(\bar{x}) = \frac{\mathcal{K}'}{24}\bar{x}^4 + \frac{c_1}{6}\bar{x}^3 + \frac{c_2}{2}\bar{x}^2 + c_3\bar{x} + c_4.$$

Likewise, for $\bar{s} \leq \bar{x} \leq 1$ the beam shape is given by

$$\frac{\epsilon}{L}\bar{w}_2(\bar{x}) = \frac{\mathcal{K}'}{24}\bar{x}^4 + \frac{c_5}{6}\bar{x}^3 + \frac{c_6}{2}\bar{x}^2 + c_7\bar{x} + c_8.$$

The eight boundary conditions required to determine the eight unknown constants $c_1, \ldots, c_8$ are as follows. At $\bar{x} = \bar{s}$, we have the matching conditions $\bar{w}_1(\bar{s}) = \bar{w}_2(\bar{s})$, $\bar{w}_{1,\bar{x}}(\bar{s}) = \bar{w}_{2,\bar{x}}(\bar{s})$ and $\bar{w}_{1,\bar{x}\bar{x}}(\bar{s}) = \bar{w}_{2,\bar{x}\bar{x}}(\bar{s})$, and the jump condition $\bar{w}_{2,\bar{x}\bar{x}\bar{x}}(\bar{s}) - \bar{w}_{1,\bar{x}\bar{x}\bar{x}}(\bar{s}) = \mathcal{K}'\mathcal{M}L/\epsilon$. At $\bar{x} = 0$, the beam is fixed ($\bar{w}_1(0) = 0$) and supported (moment free, $\bar{w}_{1,\bar{x}\bar{x}}(0) = 0$). As a consequence of the small-displacement approximation, the longitudinal displacement of the hinged end is of second-order smallness compared with the transverse deflection, and thus we may take $\bar{w}_2(1) = 0$ and $\bar{w}_{2,\bar{x}\bar{x}}(1) = 0$ (Landau & Lifshitz 1986). By solving the system of equations defined by this set of boundary conditions, the beam shape may be expressed as a function of the load position

$$\frac{\epsilon}{L}\bar{w}_1(\bar{x},\bar{s}) = \frac{\mathcal{K}'\bar{x}(\bar{x}^3 - 2\bar{x}^2 + 1 - 4\bar{x}^2\mathcal{M} + 4\bar{x}^2\bar{s}\mathcal{M} - 12\bar{s}^2\mathcal{M} + 8\bar{s}\mathcal{M} + 4\bar{s}^3\mathcal{M})}{24}$$

$$(3.9)$$

and

$$\frac{\epsilon}{L}\bar{w}_2(\bar{x},\bar{s}) = \frac{\mathcal{K}'(\bar{x}-1)(\bar{x}^3 - \bar{x}^2 - \bar{x} + 4\bar{x}^2\bar{s}\mathcal{M} - 8\bar{x}\bar{s}\mathcal{M} + 4\bar{s}^3\mathcal{M})}{24}. \quad (3.10)$$

It follows that the contact between the load and the beam occurs at the point $\bar{w}_1(\bar{s},\bar{s}) = \bar{w}_2(\bar{s},\bar{s})$. If the load is a sphere with radius R, the trajectory of its centre of mass is therefore

$$\frac{\epsilon}{L}\bar{w}_{\text{sphere}}(\bar{x}) = \frac{\mathcal{K}'\bar{x}(\bar{x}-1)(8\bar{x}^2\mathcal{M} - 8\bar{x}\mathcal{M} + \bar{x}^2 - \bar{x} - 1)}{24} - \frac{R}{L}. \quad (3.11)$$

The maximum static deflection

$$\frac{\epsilon}{L}\bar{w}\left(\frac{1}{2},\frac{1}{2}\right) = \mathcal{K}'\frac{(8\mathcal{M}+5)}{384} \quad (3.12)$$

is given by the solid curve in figure 5, which is in good agreement with the experimentally observed deflection amplitude.

By combining (3.4) and (3.5), one obtains an expression for the load dynamics

$$\left(1 + \frac{J}{mR^2}\right)\frac{\mathrm{d}^2\bar{s}}{\mathrm{d}\bar{t}^2} + \left(\frac{\epsilon}{L}\right)^2\bar{w}_{\bar{t}\bar{t}}\bar{w}_{\bar{x}}\delta(\bar{x}-\bar{s}) = \frac{gT^2}{L}\left(\frac{\epsilon}{L}\bar{w}_{\bar{x}}\delta(\bar{x}-\bar{s})\cos\theta + \sin\theta\right), \quad (3.13)$$

where we have introduced the dimensionless variables $\bar{s} = s/L$, and $\bar{t} = t/T$. Since the second term in (3.13) is of second-order smallness in ϵ/L, we may rewrite (3.13) as

$$\left(1 + \frac{J}{mR^2}\right)\frac{\mathrm{d}^2\bar{s}}{\mathrm{d}\bar{t}^2} = \frac{\epsilon}{L}\bar{w}_{\bar{x}}\delta(\bar{x}-\bar{s})\cos\theta + \sin\theta, \quad (3.14)$$

where we choose $T = \sqrt{L/g}$ for the sake of simplicity. Combining (3.14) with the $\bar{x}$ derivative of (3.9) yields

$$\left(1 + \frac{J}{mR^2}\right)\frac{\mathrm{d}^2\bar{s}}{\mathrm{d}\bar{t}^2} = \frac{\mathcal{K}'\cos\theta(2\bar{s}-1)\left(8\bar{s}^2\mathcal{M} - 8\bar{s}\mathcal{M} + 2\bar{s}^2 - 2\bar{s} - 1\right)}{24} + \sin\theta. \quad (3.15)$$

Integration of (3.15) yields an expression for the load speed

$$\left(1 + \frac{J}{mR^2}\right)\left(\frac{\mathrm{d}\bar{s}}{\mathrm{d}\bar{t}}\right)^2 = \frac{\mathcal{K}'\cos\theta\,\bar{s}(\bar{s}-1)(4\bar{s}^2\mathcal{M} - 4\bar{s}\mathcal{M} + \bar{s}^2 - \bar{s} - 1)}{12}$$

$$+ 2\bar{s}\sin\theta + \frac{C}{12}, \quad (3.16)$$

where $C = -\mathcal{K}'\cos\theta\,\bar{x}_0(\bar{x}_0 - 1)(4\bar{x}_0^2\mathcal{M} - 4\bar{x}_0\mathcal{M} + \bar{x}_0^2 - \bar{x}_0 - 1) - 24\bar{x}_0\sin\theta$ and $\bar{x}_0$ is the initial position of the load. In the quasi-static limit, the elastochrone is thus defined by

$$\tau_{\text{E}} = \int_0^1 \sqrt{\frac{12\left(1 + \frac{J}{mR^2}\right)}{\mathcal{K}'\cos\theta\,\bar{s}(\bar{s}-1)(4\bar{s}^2\mathcal{M} - 4\bar{s}\mathcal{M} + \bar{s}^2 - \bar{s} - 1) + 24\bar{s}\sin\theta}}\,\mathrm{d}\bar{s}, \quad (3.17)$$
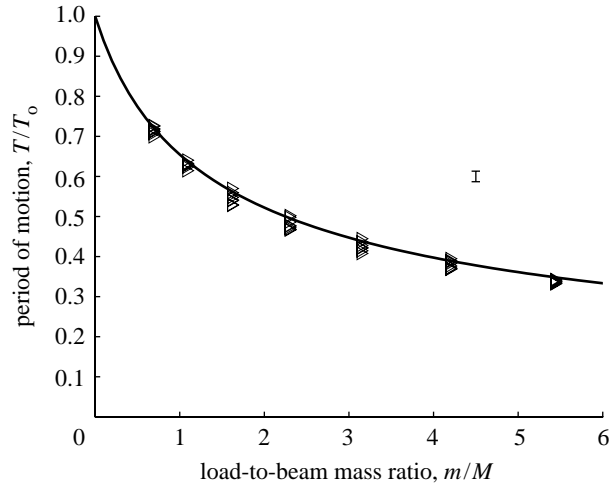
in which $\bar{x}_0 = 0$.

Figure 11. Dimensionless period of load motion versus load-to-beam mass ratio for loads released near the midpoint of an initially horizontal beam, $|x_0/L - 0.5| \leq 0.25$. The triangles denote the experimentally observed periods. The theoretically predicted period is given by the solid curve and defined by (3.19). A characteristic error bar is shown. $\mathcal{K} = 0.744$, $\theta = 0$, $T_0 = (4\pi/15)\sqrt{630}\sqrt{EI/Mg^2L}$.

(b) Horizontal beam $\theta \ll 1$

For small initial inclinations, the load motion in the quasi-static limit is described by a nonlinear oscillator, the period of which is mass dependent. The period may be approximated by considering small-amplitude oscillations about the stable equilibrium position $\bar{s} = 1/2$. If we define $\bar{s} = (1/2) + \varepsilon$, then (3.15) reduces to the pendulum equation

$$\varepsilon_{\bar{t}\bar{t}} = -\bar{\omega}^2 \varepsilon, \tag{3.18}$$

where we have neglected terms of $O(\varepsilon^2)$ and defined $\bar{\omega}^2 = (mR^2/(mR^2 + J)) \mathcal{K}(\mathcal{M}/6 + 1/8)$. The period predicted by (3.18) assumes the form

$$T^* = 4\pi\sqrt{2}\sqrt{1 + \frac{J}{mR^2}}\sqrt{\frac{EI}{Mg^2L}}\frac{1}{\sqrt{1 + \frac{4}{3}\frac{m}{M}}}, \tag{3.19}$$

which is compatible with (1.2).

We now return to the data presented in figure 7, where the dependence of the period of load motion on both the load-to-beam mass ratio and release distance is shown. If we consider only experiments for which the release distance from the beam's midpoint is less than one-quarter the beam length, and plot the period versus load-to-beam mass ratio, we obtain the data collapse shown in figure 11. The solid curve denotes the theoretically predicted period defined by (3.19).

In figure 12, we present the collapse of the period data presented in figure 7. The model adequately collapses the observed period data to T^* for loads released near the beam centre, $|x_0/L - 0.5| \leq 0.25$. For loads released substantially off centre, the period is found numerically by integrating (3.16) for various load-to-beam mass ratios, and given by the solid and dashed curves. Note that while (3.16) captures the observed upward trend in period with increasing release
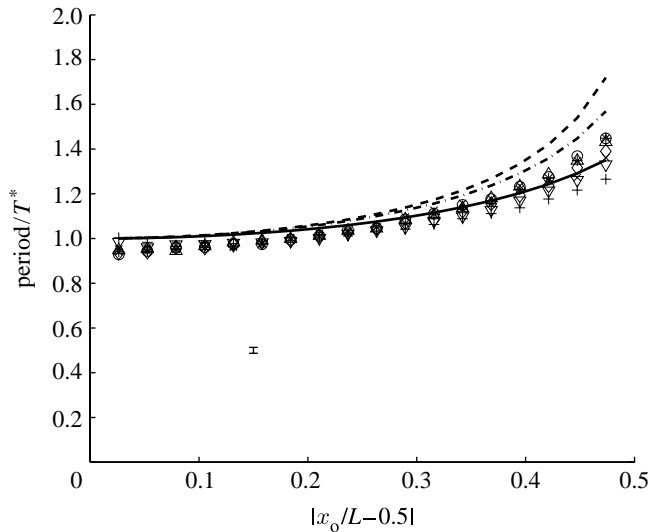
Figure 12. Collapse of the period data presented in figure 7. Dependence of the oscillation (non-dimensionalized by T^* as defined in (3.19)) on the release distance from the midpoint of an initially horizontal beam for various load-to-beam mass ratios $\mathcal{M}=m/M$: crosses, $\mathcal{M}=5.43$; up triangles, $\mathcal{M}=4.19$; circles, $\mathcal{M}=3.14$; asterisks, $\mathcal{M}=2.29$; diamonds, $\mathcal{M}=1.61$; down triangles, $\mathcal{M}=1.08$; pluses, $\mathcal{M}=0.68$. A characteristic error bar is shown.

distance, it overpredicts the period for heavy loads released near the beam's ends. The discrepancy likely arises from shortcomings of the quasi-static approximation, specifically the neglect of the beam's inertia.

(c) Inclined beam $\theta \gg 1$

Unlike in Galileo's classical study of rolling spheres along a rigid ramp, the sphere's mass affects both its trajectory and velocity when descending along a flexible beam. In particular, as the load-to-beam mass ratio $\mathcal{M}=m/M$ increases, the descent time decreases. This trend is observed in figure 9 for a particular incline, $\theta=10°$, where the theoretically predicted descent time is obtained via numerical integration of (3.16). The agreement between the theoretical prediction (solid curve) and experiment is excellent, with the exception of the data point representing the heaviest sphere. We note that in this case, the sphere loses contact with the beam (figure 8c), so (3.16) is no longer valid. For the sake of comparison, the descent time along the corresponding brachistochrone curve is given by the dashed line in figure 9. Recall that the brachistochrone curve, the curve of the fastest descent in a gravitational field, may be defined parametrically as

$$\left.\begin{aligned} \xi &= \beta(\phi - \sin\phi), \\ \eta &= \beta(1 - \cos\phi), \end{aligned}\right\} \tag{3.20}$$

where we take the origin of the Cartesian coordinate system (ξ, η) to be the upper end of the curve, with η aligned with the direction of gravity. By specifying the lower end of the curve (ξ_0, η_0), the coefficient β is found by solving numerically the relationship
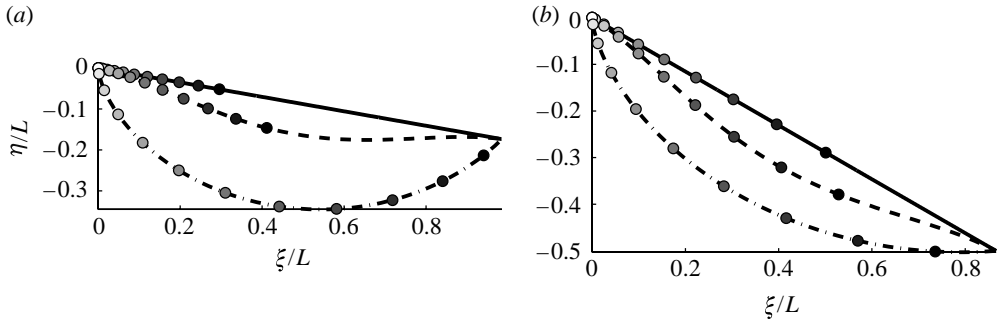
Figure 13. Predicted trajectories of a rolling point mass along a rigid ramp (solid line), a flexible beam (dashed curve, $\mathcal{K}=1$, $\mathcal{M}=3$), and a brachistochrone curve (dash-dotted curve) for (*a*) $\theta=10°$ and (*b*) $\theta=30°$. The shading denotes the positions at equal times, spaced by equal intervals $\Delta \bar{t}=0.2$.

$$\frac{\xi_0}{\eta_0} = \frac{\phi^* - \sin \phi^*}{1 - \cos \phi^*},$$

for ϕ^* and substituting the result into (3.20). The descent time along the brachistochrone curve is therefore

$$\tau_{\mathrm{B}} = \int_0^{\phi^*} \sqrt{\left(1 + \frac{J}{mR^2}\right) \frac{\xi^2 + \eta^2}{2g\eta}} \, \mathrm{d}\phi = \phi^* \sqrt{\left(1 + \frac{J}{mR^2}\right) \frac{\eta_0}{g(1 - \cos \phi^*)}}. \quad (3.21)$$

The elastochrone tends towards the brachistochrone as $\mathcal{M}$ increases (figure 9). However, if the two ever intersect, it would be at a load-to-beam mass ratio beyond that consistent with the quasi-static approximation, for which (1.4) is not satisfied, and (3.16) cannot be reliably used to determine the descent time. In fact, the brachistochrone can never exceed the elastochrone.

Consider the path P taken by a sphere descending a flexible beam between two points in a gravitational field. Let P' be the same path taken by a sphere along a rigid ramp. At each point along P', the kinetic energy of the sphere will exceed that along P by an amount equal to the sum of the bending and kinetic energies of the beam, both non-negative quantities. Therefore, the elastochrone is bounded from below by the descent time along a rigid ramp that yields the same trajectory, that is in turn bounded from below by the brachistochrone.

A comparison between the brachistochrone and elastochrone curves is shown in figure 13 for 10° and 30° initial inclinations, where we present the trajectories of a rolling point mass for a particular $\mathcal{M}$ and $\mathcal{K}$. In both cases, descent along the brachistochrone curve is faster than that along the elastochrone curve, as illustrated by the shaded circles separated by equal time intervals $\Delta \bar{t} = 0.2$. The trajectory along a Galilean ramp is also included for the sake of comparison.

(*d*) *Inertial effects*

The inertial effects of load motion are twofold. First, the load's inertia may augment the gravitational loading, and so give rise to additional deflection. Second, the beam's inertia may generate bending waves as the load rolls. For a beam of uniform mass density M/L, the dispersion relationship is given by

$$\omega = k^2\sqrt{\frac{EIL}{M}}, \qquad (3.22)$$

where k is the wavenumber and ω the angular frequency (Landau & Lifshitz 1986). Using a wavelength $\lambda = 2\pi/k = 2L$, the value predicted by (3.22), $5.8\,\mathrm{s}^{-1}$, is consistent with that observed in figure 4. The observed decrease in vibration frequency with increasing load mass reported in §2 may be roughly understood by reconsidering a beam of uniform mass density $(m+M)/L$.

In §3a, we demonstrated that the beam's inertia is negligible in the quasi-static limit (1.4). We then considered the limit in which the load's inertia is also negligible (1.5), and so obtained an expression for the load trajectory (3.11) and load speed (3.16). We here extend our theoretical model to include the load's inertia by using our results from §3a to approximate the load dynamics.

The load's inertia becomes important in the beam-and-mass dynamics when gravitational and inertial loadings are comparable, specifically, when $\mathcal{F} \sim O(1)$. The inertial loading is encompassed by the total differential in (3.2), which may be expanded to yield

$$\frac{\mathrm{d}^2 w(s,t)}{\mathrm{d}t^2} = w_{tt} + 2w_{tx}\frac{\mathrm{d}s}{\mathrm{d}t} + w_{xx}\left(\frac{\mathrm{d}s}{\mathrm{d}t}\right)^2 + w_x\frac{\mathrm{d}^2 s}{\mathrm{d}t^2}. \qquad (3.23)$$

To derive the corrected beam shape $\tilde{w}$, we include (3.23) in the jump condition, use (3.9) and (3.10) to approximate the beam shape, (3.15) to approximate the load acceleration and (3.16) its speed, and proceed as in §3a. Rather than presenting the lengthy result here, we instead present the maximum dynamic deflection for $J = 2/5$, and $\theta = 0$:

$$\frac{\epsilon}{L}\tilde{w}\left(\frac{1}{2},\frac{1}{2}\right) = \frac{\epsilon}{L}\bar{w}\left(\frac{1}{2},\frac{1}{2}\right) + \frac{25}{516\,096}\mathcal{K}^3\mathcal{M} + \frac{5}{36\,864}\mathcal{K}^3\mathcal{M}^2 + \frac{5}{64\,512}\mathcal{K}^3\mathcal{M}^3,$$
$$\qquad (3.24)$$

corresponding to the parameters of the experiment presented in figure 3. The deflection amplitude predicted by (3.24) is given by the dashed curve in figure 5, and provides a small improvement to that predicted by (3.12), the derivation of which neglected load inertia. The observed dependence of the vibration amplitude on the mass ratio is shown in figure 6. The dependence may be understood by considering the increased deflection caused by the inertial loading, $\tilde{w} - \bar{w}$, given by the solid line.

The influence of the inertial loading on the sphere dynamics is readily determined by substituting $\tilde{w}_x$ for $\bar{w}_x$ in (3.14). For $J = 2/5$, $\theta = 0$ and $0 \le \bar{x}_0 \le 1$, we numerically integrate the resulting equation for load-to-beam mass ratios 0.68, 2.29 and 5.43. The theoretically predicted descent times are plotted in figure 12 and are indistinguishable from those predicted without consideration of the load's inertia. We thus conclude that the discrepancy between experiment and theory apparent in figure 12 cannot be attributed to the neglect of the load's inertia alone, but probably arises from the neglect of the beam inertia.

4. Discussion

We have presented the results of a combined theoretical and experimental investigation of the dynamic behaviour of flexible beams subjected to moving loads with deflection-dependent acceleration. We first observe that heavy loads traverse the beam faster than light loads owing to the coupling between the load mass and beam deflection. For initially horizontal beams, an oscillatory motion takes place, the period of which decreases with increasing load mass, unlike for a simple pendulum.

We have rationalized the observed behaviour by developing a theoretical model for the beam-and-mass dynamics based on Euler–Bernoulli beam theory. In the quasi-static limit, we obtain an exact expression for the load trajectory and a simple expression for its velocity, both of which are found to be in excellent agreement with experiment. For an initially horizontal beam with $\mathcal{K} = MgL^2/EI = 0.744$, our theoretical model reasonably predicts the period of load motion for load-to-beam mass ratios $\mathcal{M} = m/M < 3$. For $\mathcal{M} > 3$, the discrepancy may be attributed to shortcomings of the quasi-static approximation, which neglects the kinetic energy of the beam. While the small-slope approximation provides a potential source of error, numerical results indicate that this error accounts for less than 1% of the observed difference in descent times between experiment and theory for $\mathcal{M} \leq 6$. Finally, we have demonstrated that the descent time along a flexible beam, the elastochrone, always exceeds the classical brachistochrone.

There are several outstanding questions that warrant further consideration. While our theoretical model provides a first approximation for the load motion in the regime in which the quasi-static assumption breaks down, it overpredicts the period of motion. A more sophisticated model would entail consideration of the influence of beam vibrations on the load motion. Finally, while separation between a load moving at constant speed and its supporting structure was considered by Lee (1998), the general case in which the load motion is deflection dependent has yet to be investigated.

Appendix A. Small-slope approximation

We here consider the range of validity of the small-slope approximation, $w_x \ll 1$, for determining the quasi-static shape of the beam. In the quasi-static limit, the shape of an Euler–Bernoulli beam with arbitrarily large slopes may be solved numerically using the shooting method. We do so for the beam used in the experimental study, and present the predicted deflection amplitude versus load-to-beam mass ratio as the dash-dotted curve in figure 14. For comparison, the predicted deflection amplitude in the small-slope, quasi-static limit is given by the solid curve. For load-to-beam mass ratios $m/M < 10$, the error due to the small-slope approximation is negligible. Moreover, both predictions are in excellent agreement with a series of experiments wherein each of the nine spheres was placed statically at the beam's midpoint and its deflection amplitude measured.
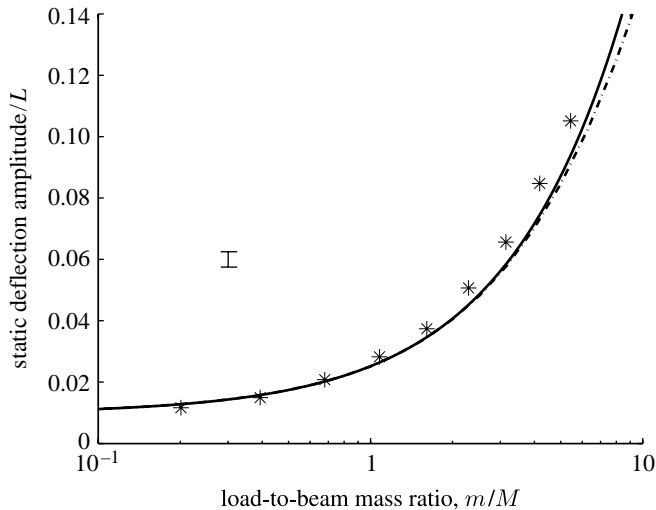
Figure 14. Dimensionless static deflection amplitude versus load-to-beam mass ratio m/M for an initially horizontal beam. The asterisks denote the experimentally observed beam deflections. The solid curve denotes the small-slope approximation and is defined by (3.12). The dash-dotted curve denotes the numerical solution to the nonlinear beam equation in the quasi-static limit. A characteristic error bar is shown.

References

Anon 1697 Commonly attributed to I. Newton. *Phil. Trans.* **19**, 388.

Blinov, A. P. 2008 The motion of a point mass along a string. *J. Appl. Math. Mech.* **72**, 12–14. (doi:10.1016/j.jappmathmech.2008.03.005)

Bolotin, V. V. 1961 Problem of bridge vibration under the action of a moving load. *Izvestiya AN SSSR, Mekhanika I Mashinostroenie* **4**, 109–115.

Boyer, C. B. & Merzbach, U. C. 1991 *A history of mathematics*, 2nd edn. New York, NY: Wiley.

Davys, J. W., Hosking, R. J. & Sneyd, A. D. 1985 Waves due to a steadily moving source on a floating ice plate. *J. Fluid Mech.* **159**, 269–287. (doi:10.1017/S0022112085002646)

Derendyayev, N. V. & Soldatov, I. N. 1997 The motion of a point mass along a vibrating string. *J. Appl. Math. Mech.* **61**, 681–684. (doi:10.1016/S0021-8928(97)00086-5)

Flaherty Jr, F. T. 1968 Transient resonance of an ideal string under a load moving with varying speed. *Int. J. Solids Struct.* **4**, 1221–1231. (doi:10.1016/0020-7683(68)90006-1)

Fryba, L. 1972 *Vibration of solids and structures under moving loads*. Prague, Czech Republic: Academia Publishing House.

Galilei, G. 1638 *Discorsi e dimostrazioni matematiche, intorno a due nuove scienze*. Leiden, The Netherlands: Elsevier.

Hosking, R. J., Sneyd, A. D. & Waugh, D. W. 1988 Viscoelastic response of a floating ice plate to a steadily moving load. *J. Fluid Mech.* **196**, 409–430. (doi:10.1017/S0022112088002757)

Kerr, A. D. 1976 The bearing capacity of floating ice plates subjected to static or quasistatic loads. *J. Glaciol.* **17**, 229–268.

Krylov, A. N. 1905 *Mathematical collection of papers of the Academy of Sciences*, vol. 61. (Matematischeskii sbornik Akademii Nauk). Peterburg, Russia. [Transl. Kriloff, A. N. 1905 Über die erzwungenen Schwingungen von gleichformigen elastischen Staben. *Mathematische Annal.* **61**, 211–234. (doi:10.1007/BF01457563)]

Landau, L. D. & Lifshitz, E. M. 1986 *Theory of elasticity*. Course of theoretical physics, vol. 7. Oxford, UK: Pergamon Press.

Lee, H. P. 1995 On the dynamic behaviour of a beam with an accelerating mass. *Arch. Appl. Mech.* **65**, 564–571. (doi:10.1007/BF00789097)

Lee, U. 1998 Separation between the flexible structure and the moving mass sliding on it. *J. Sound Vib.* **209**, 867–887. (doi:10.1006/jsvi.1997.1287)

Lowan, A. N. 1935 On transverse oscillations of beams under the action of moving variable loads. *Philos. Mag. Ser. 7* **19**, 708–715.

Michaltsos, G. T. 2002 Dynamic behaviour of a single-span beam subjected to loads moving with variable speeds. *J. Sound Vib.* **258**, 359–372. (doi:10.1006/jsvi.2002.5141)

Nevel, D. E. 1970 Moving loads on a floating ice sheet. US Army CRREL research report 261.

Rodeman, R., Longcope, D. B. & Shampine, L. F. 1976 Response of a string to an accelerating mass. *J. Appl. Mech.* **14**, 675–680.

Sagartz, M. J. & Forrestal, M. J. 1975 Motion of a stretched string loaded by an accelerating force. *J. Appl. Mech.* **13**, 505–506.

Schallenkamp, A. 1937 Schwingungen von tragern bei bewegten lasten. *Ingenieur-Archiv.* **8**, 182–198. (doi:10.1007/BF02085995)

Smith, C. E. 1964 Motions of a stretched string carrying a moving mass particle. *J. Appl. Mech.* **31**, 29–37.

Squire, V. A., Hosking, R. J., Kerr, A. D. & Langhorne, P. J. 1996 *Moving loads on ice plates.* Dordrecht, The Netherlands: Kluwer Academic Publishers.

Steuding, H. 1934 Die Schwingungen von tragern bei bewegten lasten. *Ingenieur-Archiv.* **1–2**, 275–305. (See also pp. 265–270.)

Stokes, G. 1849 Discussion of a differential equation relating to the breaking of railway bridges. *Trans. Camb. Philos. Soc.* (*Part 5*) **8**, 707–735. (Reprinted in *Mathematical and Physical Papers* **1883**, 178–220.)

Strathdee, J., Robinson, W. H. & Haines, E. M. 1991 Moving loads on ice plates of finite thickness. *J. Fluid Mech.* **226**, 37–61. (doi:10.1017/S0022112091002288)

Timoshenko, S. P. 1908 [Forced vibration of prismatic bars]. Izvestiya Kievskogo Politekhnicheskogo Instituta. [In Russian.] [Transl. Erzwungene Schwingungen prismatiseher stäbe. *Zeitsch. F. Mathematik u. Physik* 1911, **59**, 163–203.]

Timoshenko, S. P. 1953 *History of the strength of materials.* New York, NY: D. van Nostrand Co.

Willis, R. *et al.* 1849 Experiments for determining the effects produced by causing weights to travel over bars with different velocities. In *Report of the commissioners appointed to inquire into the application of iron to railway structures* (eds G. Grey *et al.*). London, UK: W. Clowes and Sons. (Reprinted in: Barlow, P. 1851 Treatise on the strength of timber, cast iron and malleable iron. London.)

Zimmermann, H. 1896 Die schwingungen eines tragers mit bewegter lasts. *Centralblatt der Bauverwaltung* **16**, 249–251. (See also pp. 257–260, 264–266, 288.)